Real-time estimates of the ICRF single-pass absorption for ITER

Ernesto Lerche[1*], *Dirk* Van Eester[1], *Mireille* Schneider[2], *Pierre* Dumortier[1], *Philippe* Lamalle[1], *Walid* Helou[2], *Ivo* Carvalho[2], and *Anna* Vu[2]

[1] *Laboratory for Plasma Physics, ERM/KMS, B-1000 Brussels, Belgium*
[2] *ITER Organization, Route de Vinon-sur-Verdon, CS 90 046, 13067 St. Paul-lez-Durance Cedex, France*

Abstract. Estimating the single-pass absorption (SPA) of a given Ion Cyclotron Resonance Heating (ICRH) scenario as function of the plasma and the radio-frequency (RF) wave properties requires a multi-species hot plasma wave solver. Even in 1D and using truncated finite Larmor radius expansion for the plasma dielectric response, the simulations cannot be done much faster than in a couple of seconds. In ITER, it is envisaged to estimate the single-pass absorption of the ICRF waves in real-time to take preventive actions in case of poor absorption for avoiding increased plasma-wall interaction and enhanced heat loads on the plasma facing components. This work proposes a potential solution based on pre-calculated look-up tables of the ICRF single-pass absorption that can be interpolated in real-time by the Advanced Protection System (APS) and by the Plasma Control System (PCS) in ITER [1,2,3] during the discharge evolution. The tables can also be used as input for the Pulse Design Simulator (PDS) [4] and other modelling tools that require the ICRF absorption information for control and/or protection. The SPA tables are produced as function of the dominant parameters governing the RF wave propagation and absorption using the 1D TOMCAT code [5] for some ITER-relevant ICRH scenarios.

1 Introduction

The single-pass absorption (SPA) of a wave injected in the plasma is a figure of merit of the heating efficiency of a particular heating scheme. For Ion Cyclotron Resonance Heating (ICRH), global SPA values above 50% usually indicate a good absorption scheme, since the waves are reflected in a cut-off layer at the plasma high-field side and are reabsorbed in their way back through the plasma, effectually leading to a suitable heating efficiency. In ITER, it is proposed to calculate the SPA in real time, to either regulate the ICRF power when the conditions are not favourable for the wave absorption or to tune the ICRF scenario for a particular task, e.g. producing ion heating for easier H-mode access [6] or turbulence suppression [7], electron heating for impurity screening [8,9] or fast ion generation for sawtooth control [10,11]. However, even using the simplest models required for a meaningful estimation of the SPA in ITER, calculating it in real-time (1-2ms) remains extremely challenging.

In this work, we propose an alternative solution for this task, namely pre-calculating the SPA of a given ICRH scenario as function of the main parameters that govern its magnitude, store this information in multi-dimensional look-up tables and interpolate the tables in real-time during the actual discharge execution. Using the 1D ICRH TOMCAT code [5], 3-dimensional SPA tables are produced as function of the central plasma density N_0, the central plasma temperature T_0 and the minority (H or ^{3}He) concentration $X_{min} = n_{min}/n_e$ for the main ICRH scenarios foreseen in ITER, both at half-field ($B_0 = 2.65$T) and at full-field ($B_0 = 5.3$T). For each case, a frequency range of ± 2MHz around the nominal frequency and three different phasing configurations are considered. Parabolic kinetic profiles are imposed and we assume $T_i = T_e/2$, since dominant electron heating is expected in ITER. Table 1 shows the summary of the various ICRH scenarios investigated. In general, the equilibrium magnetic field B_0, the plasma composition and minority species (scenario) and the antenna phasing (phases) are constant (prescribed before the discharge) and the RF frequency can vary by a maximum of 2MHz. Thus, the main changes in the SPA values to be accounted for in the real-time interpolation during the discharge evolution will effectively be contained in the 3D tables given as function of N_0, T_0 and X_{min}, with small variations to adjust for eventual frequency changes.

Table 1. Summary of the 3D SPA tables compiled for 4 different ICRH scenarios foreseen in ITER

Scenario	B_0 (T)	f (MHz)	phases	N_0, T_0, X_{min}
(H) D	2.65T	40-44	$0\pi\pi0$, $0\pi0\pi$ $0\frac{\pi}{2}\pi\frac{3\pi}{2}$	3D
(^{3}He) H	5.3T	50-54	$0\pi\pi0$ $0\pi0\pi$ $0\frac{\pi}{2}\pi\frac{3\pi}{2}$	3D
(^{3}He) D	5.3T	50-54	$0\pi\pi0$ $0\pi0\pi$ $0\frac{\pi}{2}\pi\frac{3\pi}{2}$	3D
(^{3}He) DT	5.3T	50-54	$0\pi\pi0$ $0\pi0\pi$ $0\frac{\pi}{2}\pi\frac{3\pi}{2}$	3D

* Corresponding author: Ernesto.Lerche@mil.be

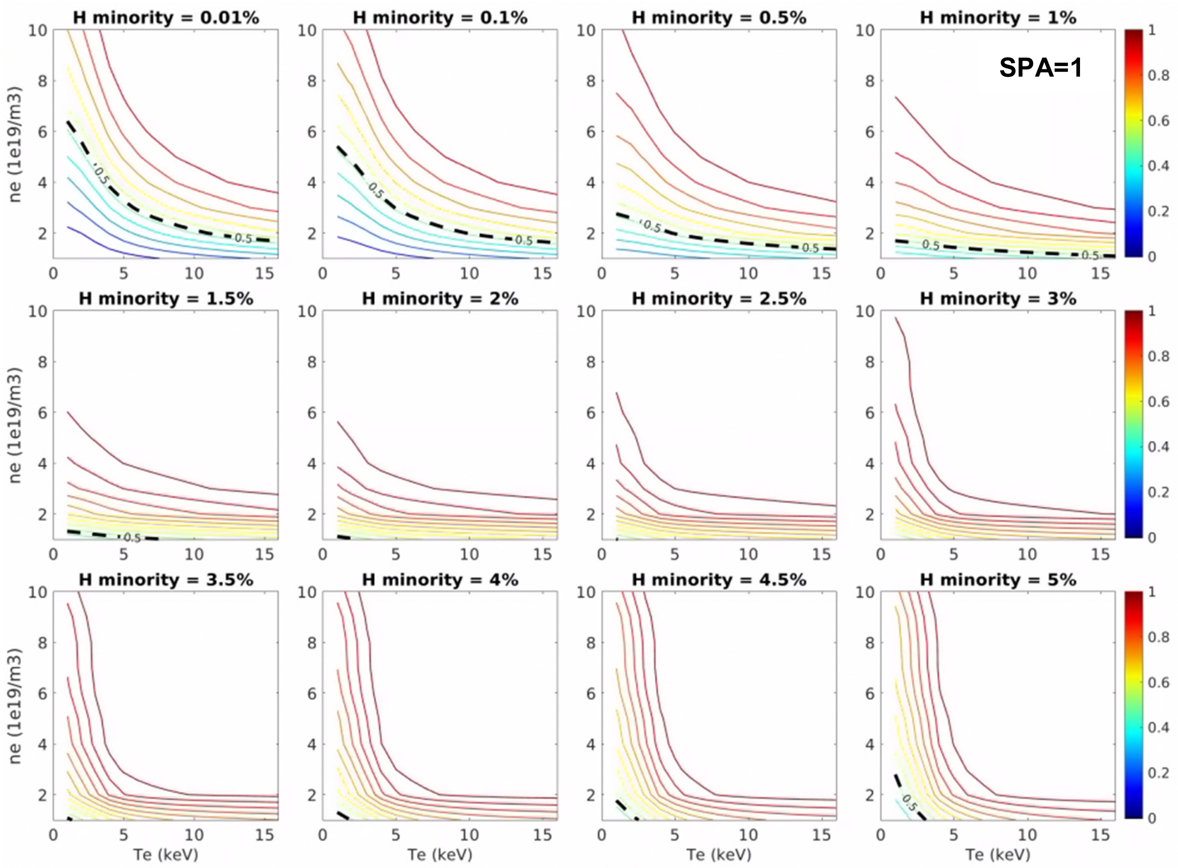

Fig. 1. 3D single-pass absorption (SPA) tables for H minority heating in D plasmas with B_0=2.65T, *f*=40MHz and phase=0ππ0.

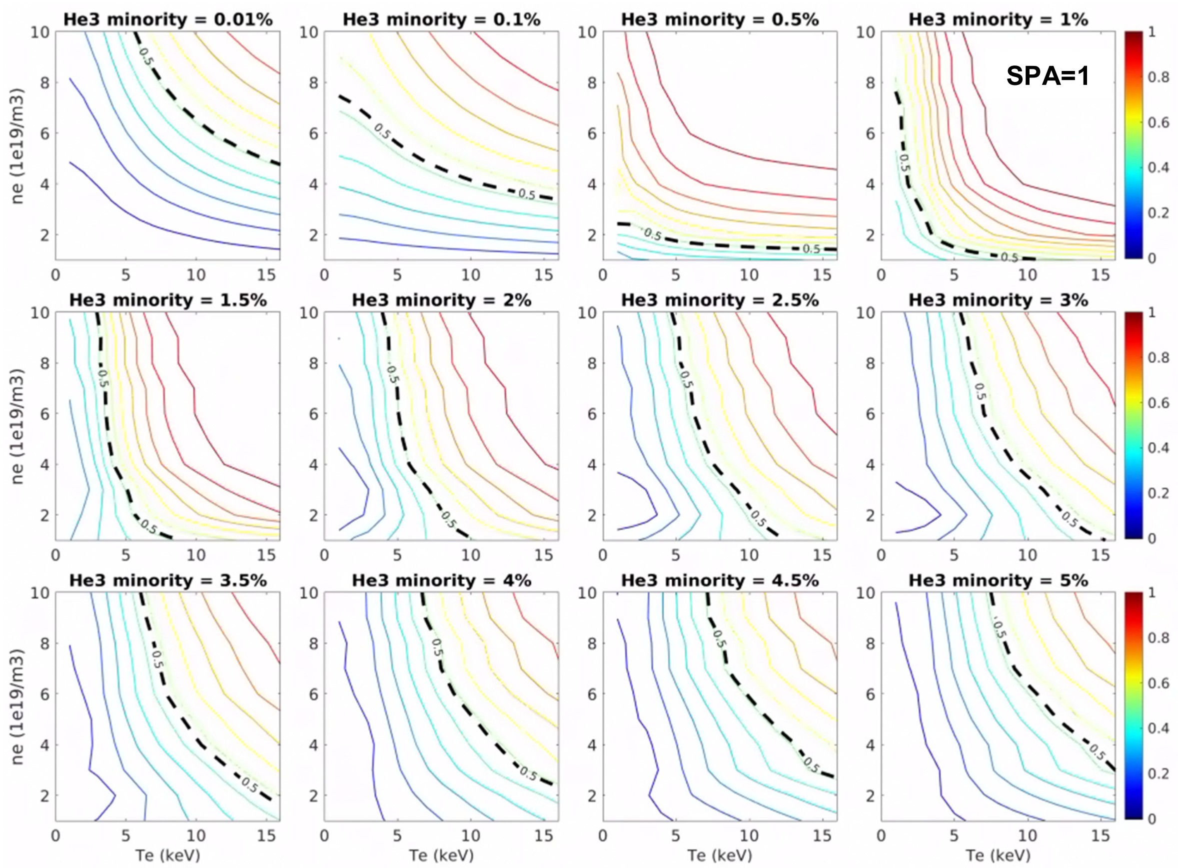

Fig. 2. 3D single-pass absorption (SPA) tables for ^{3}He minority heating in D-T plasmas with B_0=5.3T, *f*=52MHz and phase=0ππ0.

2 Results & Discussion

Figures 1 and 2 show, respectively, the 3D single-pass absorption look-up tables computed for H minority ICRH in D plasmas (B_0 = 2.65T, f = 40MHz, 0ππ0) and for ^{3}He minority ICRH in D-T plasmas (B_0 = 5.3T, f = 52MHz, 0ππ0). Each panel shows the SPA contours as function of the central plasma density (N_0) and electron temperature (T_0) values at a given minority concentration $X_{min} = n_{min}/n_e$. The black dashed lines indicate the isolines with SPA=0.5. For the H minority heating case, full absorption (SPA=1) is predicted in a wide range of the parameter space explored, with exception to the low density and temperature regions when the minority concentration is below $X_{min} < 1\%$. The ^{3}He minority heating scenario in D-T also shows large areas of large SPA, in particular at high values of N_0 and T_0, but the low absorption domain is broader than for the H minority heating case. For example, at larger ^{3}He concentrations ($X_{min} > 2\%$), the low temperature domain exhibits limited SPA even at high plasma density. The low absorption region is extended when the ^{3}He concentration is larger. The panels with X_{min} = 0.01% (no minority injection) in Fig.1 and Fig.2 represent, respectively, the Deuterium and Tritium absorption by second harmonic ($\omega = 2\omega_c$) ICRF heating, which are more efficient at high densities and at high temperatures. The $\omega = 2\omega_c$ T heating case at low N_0, T_0 values (e.g. in L-mode) is particularly limited and requires ^{3}He injection to become efficient in these conditions.

For the calculations of Figs. 1 and 2, the minority species are resonant near the plasma centre but are not necessarily the dominant absorbing species in all cases. Electron absorption via Landau damping (LD) and transit-time magnetic pumping (TTMP) is always present and can exceed 50% of the total absorption if the electron temperature is high enough.

Examples of the power absorption profiles obtained for the H minority heating scheme in D plasmas with dominant H absorption (a) and dominant electron absorption (b) are given in Fig. 3. Despite the same H concentration (X_{min} = 3%) and full SPA in both cases, at lower temperature the H absorption in the plasma centre is largely dominant while in the higher temperature case the broad off-axis electron absorption becomes the main player. The fact that the RF waves can be strongly absorbed by LD/TTMP before reaching the cyclotron layer in fusion-relevant plasmas is well known and ways to minimize this effect consist in shifting the IC resonance layer off-axis (reducing the RF frequency) and in tuning the antenna phasing configuration (reducing $k_{//}$) as discussed in [12].

Examples of the absorption profiles for the ^{3}He minority / $\omega = 2\omega_c$ T heating scenario in D-T L-mode plasma conditions (low N_0, T_0) are given in Fig.4, illustrating the importance of ^{3}He injection on the ICRF heating performance at low plasma temperatures: (a) No ^{3}He injection; (b) 1% ^{3}He. In these conditions, the SPA increases from SPA=0.19 to 0.82 with dominant ^{3}He heating when even small amounts of ^{3}He are injected.

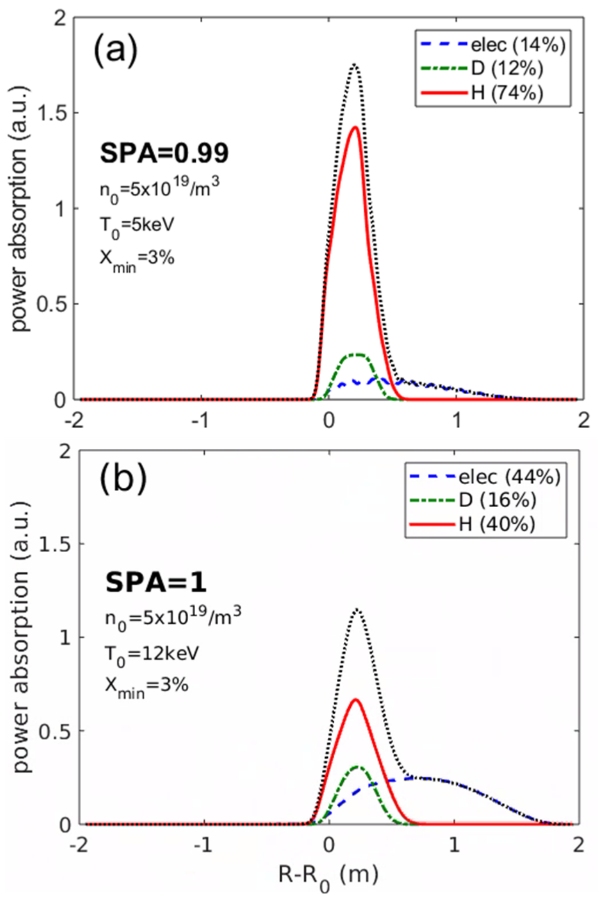

Fig. 3. Power absorption profiles for H minority heating in D plasmas (B_0=2.65T, f=40MHz, 0ππ0): (a) Low temperature case, T_0=5keV; (b) High temperature case T_0=12keV.

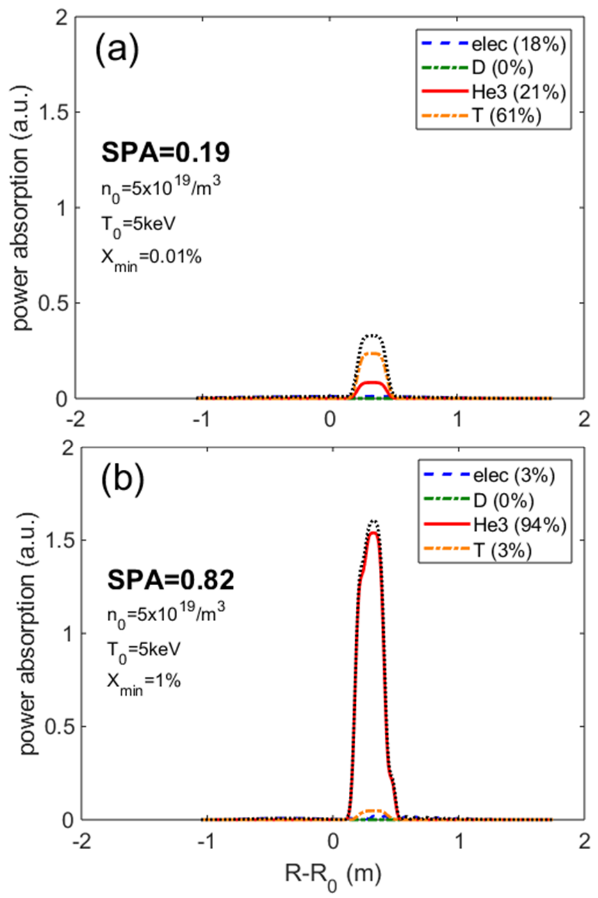

Fig. 4. Power absorption profiles for ^{3}He minority / $\omega = 2\omega_c$ T heating in D-T plasmas at low N_0, T_0 (B_0=5.3T, f=52MHz, 0ππ0): (a) No ^{3}He injection, (b) X_{min}=1%.

The legends in Figs. 3 and 4 indicate the relative power absorption of each species.

Another example of the ^{3}He / T heating scheme in D-T plasmas is given in Fig.5. Here, H-mode conditions are considered (high N_0, T_0) and a case without ^{3}He injection (a) is compared with a case with traces of ^{3}He (b) and a case with 1% ^{3}He injection (c). In these conditions, the three scenarios exhibit good SPA but while the minority ^{3}He absorption is dominant when 1% of ^{3}He is injected (c), $\omega = 2\omega_c$ T absorption is the main player when no or small traces of ^{3}He are present in the plasma. Electron heating via LD/TTMP is always significant due to the large electron temperatures assumed for these cases, $T_0 = 15$keV.

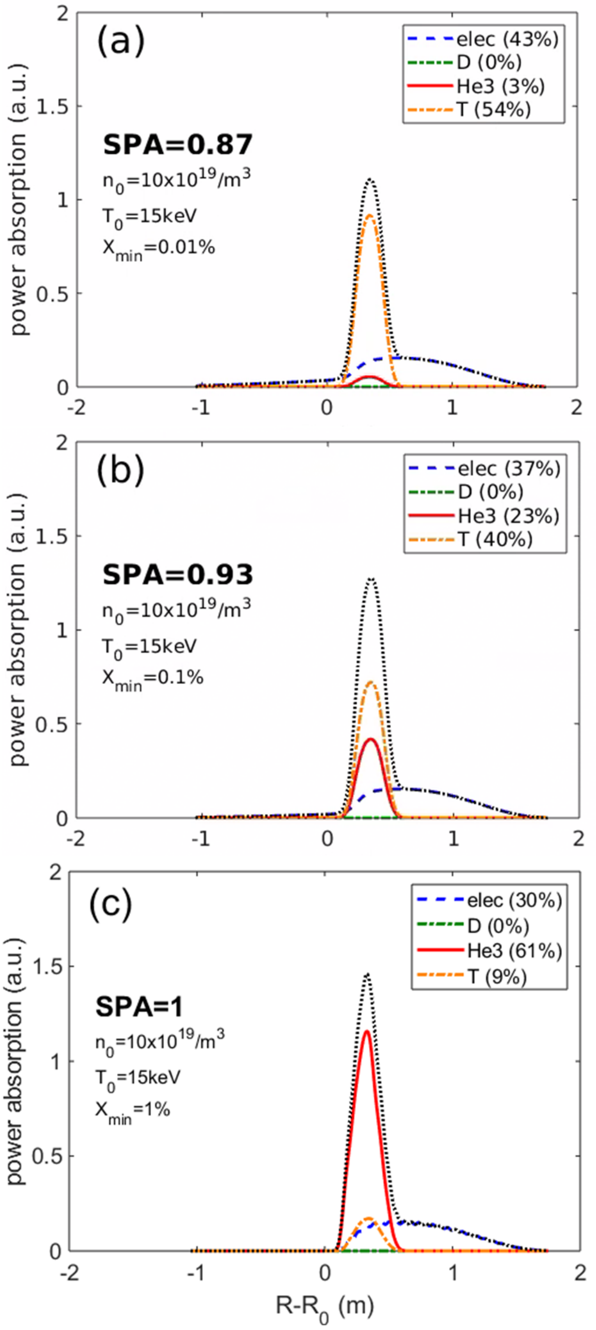

Fig. 5. Power absorption profiles for ^{3}He minority / T heating in D-T H-mode plasmas at high N_0, T_0 (B_0=5.3T, f=52MHz, 0ππ0): (a) No ^{3}He injection, (b) X_{min}=0.1%, (c) X_{min}=1%.

The results shown in Fig.5 are in line with the original ICRF heating strategy proposed for this heating scheme in ITER already long time ago [13], namely start with dominant ^{3}He heating while the plasma is cold (e.g. L-mode) and stop the ^{3}He injection once the conditions are favourable for efficient $\omega = 2\omega_c$ T heating.

Note that small amounts of ^{3}He (~1%) are sufficient to obtain dominant minority ^{3}He absorption and even when only traces are left in the plasma (0.1%), its absorption is still non-negligible. It's worthwhile noting that even if ^{3}He would not be injected at all, traces of ^{3}He will be present in the ITER D-T plasmas due to the natural T decay, as observed in the recent JET D-T experiments and reported in [14]. All the power absorption profiles shown in Figs. 3-5 are in arbitrary units but use the same normalization factor, so can be directly compared with each other.

For each heating scenario and given N_0, T_0 and X_{min} parameters, the full TOMCAT calculation (RF fields, power absorption profiles and SPA per species) takes about 0.5 sec, still quite fast for a realistic wave solver but too slow to be used in real-time. The time needed to produce a full 3D SPA table with 1920 points (N_0 = 1-10x10^{19}/m^3, T_0 = 1-16keV, X_{min} = 0.01-5%) at given magnetic field, frequency and phasing (as in Figs. 1 and 2) is ~18 min in the ITER SDCC cluster. It has to be noticed that the procedure can be easily parallelized so that the total time to produce a full 3D table set can be significantly reduced in practice. Interpolating the 3D tables takes less than 1ms at fixed frequency and about 1ms if frequency variations are accounted for, adequate for real-time interpolation by the ITER control systems.

The main ITER systems concerned in the ICRF SPA real-time estimates are the Advanced Protection System (APS) [1] and the Plasma Control System (PCS) [2,3]. The former is designed for machine protection so it is only concerned about avoiding the low SPA regions of a given ICRF heating scheme. In that sense, SPA tables as shown in Fig.1 and Fig.2 provide all the needed information and are ready to be used as such. For the PCS, the scope is broader since it aims at having the ability to control the auxiliary heat sources to tune the plasma performance according to the discharge needs. For example, to achieve H-mode more easily, bulk ion heating with ICRH may be preferrable [6] while assisting on the plasma termination may require dominant electron heating [15]. These regimes can be achieved by tuning the minority concentration, the ICRF power and the RF frequency (resonance position). Hence, for PCS, the information given in the 3D SPA tables is not enough. To assess the collisional heating properties of an ICRH scheme, a Fokker-Planck solver needs to be applied to the ICRF power absorption profiles provided by the TOMCAT calculations. For minority heating cases with moderate ion tails, a simple Stix-like Fokker-Planck solver [16, 17] is likely enough to represent the main bulk heating properties of ICRH. The fraction of the power absorbed by bulk ions and electrons will, nevertheless, depend on the level of applied ICRF power, thus adding another dimension to the 3D SPA table representation discussed here.

An illustration of the 3D SPA table interpolation results for a hypothetical D-T discharge evolution with

^{3}He min. ICRH is given in Fig.6 (d), together with the input waveforms of the central plasma density N_0 (a), central temperature T_0 (b) and ^{3}He concentration (c). During the initial 'L-mode' phase of the discharge (1), the SPA is very low and ICRF should not be applied in these conditions. In phase (2), still in 'L-mode', ^{3}He is injected up to 1% and the SPA increases very fast and reaches SPA ~ 0.8, even if the N_0 and T_0 values remain modest. In this phase ICRH could be applied without any restrictions. Phase (3) represents a transition into 'H-mode' where the plasma density and temperature are increased. The SPA increases even further and reaches SPA=1 in the H-mode flat-top (4). At this point, the ^{3}He injection is stopped and the ^{3}He content in the plasma decreases from 1% to 0.1% but the SPA remains large, because of the higher N_0 and T_0 values considered for the H-mode phase. Here, again, ICRH can be used without power nor phasing restrictions. During the 'H-mode' exit (5), the SPA decreases as the N_0 and T_0 values are reduced. Finally, during the plasma termination phase (6), the SPA is below 0.5 but still higher than in the beginning of the discharge (1), because it was assumed that the background ^{3}He levels are higher (0.1% instead of 0.01%) at the end of the discharge since ^{3}He is poorly pumped. In this case ICRH can be used to assist on the plasma termination but the coupled power should probably be moderated.

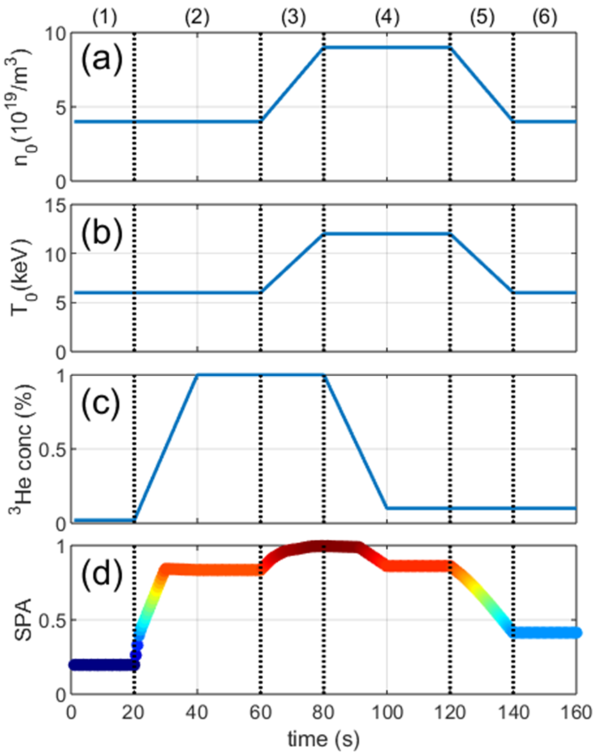

Fig. 6. Example of a simulated 'real-time' interpolation of the 3D SPA tables shown in Fig.2 for ^{3}He minority ICRH in D-T plasmas (B_0=5.3T, f=52MHz, 0ππ0): (a) Central density; (b) Central temperature; (c) ^{3}He concentration; (d) Interpolated SPA values.

In the discharge illustration depicted in Fig.6, the APS system could, for example, inhibit the ICRF power application in phase (1) and limit the ICRF power to a predefined value in phase (6) in order to avoid excessive plasma-wall interaction induced by low ICRF wave absorption. The actual ICRF power values (and other ICRF settings) to be used in the different phases of the discharge depend on a complex combination of various plasma requirements and shall be controlled by the PCS, which needs more information on the ICRF heating properties than the global SPA tables reported here, as mentioned before. This discussion is left for a future publication.

3 Summary and Conclusion

A simple procedure to estimate the single-pass absorption (SPA) of a given ICRF heating scheme in real-time in view of ITER operations has been presented. It is based on generating multi-dimensional SPA tables for the given ICRH scenario as function of the equilibrium magnetic field, the RF frequency, the antenna phasing configuration and, in particular, the plasma density, temperature and minority concentration. These tables can then be interpolated in real time by the ITER control and operation systems that require this information, such as the Advanced Protection System (APS) [1] and the Plasma Control System (PCS) [2-3]. Despite the several approximations used in the proposed procedure, the results are good enough to allow the identification of regions with poor absorption of the RF wave. High power ICRH operation in these conditions should be avoided since they would cause enhanced plasma-wall interaction and would not produce efficient plasma heating. The APS system could regulate the ICRH power (or cut it altogether) if such conditions are achieved in the discharge. Two ICRH scenarios were discussed as example: H minority heating in D plasmas at half-field (2.65T/42MHz, to be used in the non-active operation phase) and minority ^{3}He heating in D-T plasmas at full-field (5.3T/52MHz, the reference ICRH scenario for D-T operations). In both cases, large SPA is observed in most of the N_0 x T_0 parameter space at various minority concentrations ranging from 0-5%. The regions with poorest wave absorption are generally plasmas with low N_0 and T_0. This poor absorption domain is larger for the ^{3}He minority heating case than for the H min. case, in particular for ^{3}He concentrations larger than 2%. The importance of injecting small amounts of ^{3}He in low density and temperature plasmas (such in L-mode) are also highlighted.

Although the SPA tables presented here are enough input for the APS system – which is mainly concerned about safe operation of the tokamak and the auxiliary heating schemes -, they don't contain enough data to be used by the PCS controller. The latter also needs information about the collisional bulk ion and electron heating produced by ICRH in given conditions and thus requires an additional step in the calculations, namely a Fokker-Planck solver. This can be rather easily implemented but the actual procedure and tabulation strategy is still under discussion, since the applied ICRF power enters as an additional dimension in the look-up tables. Furthermore, the Pulse Design Simulator (PDS) being developed for ITER [4] also requires detailed information about the ICRF heating properties, including the 1D collisional heating profiles to be used in the associated transport solvers. As a matter of fact, most of the ICRF tools required for this task are already implemented in the H&CD PDS platform in ITER [18] but, being more sophisticated than the simple TOMCAT model proposed here, require considerably more time for the calculations. Nevertheless, it could be envisaged to extract the SPA and collisional ion/electron heating information from these calculations to produce the look-up tables necessary for the PCS system or for other control models being tested for ITER [19, 20]. It is also being assessed whether the SPA tables could be used to train a neural-network procedure to be implemented in APS and PCS for the real-time estimates of the ICRH SPA during a discharge. The advantage would be that, if well trained, such a technique could allow estimating the SPA in conditions that have not been foreseen in advance.

Finally, it's important mentioning that, on top of the SPA, the ICRF coupling resistance is another key figure of merit for regulating the ICRF power applied during the plasma discharge. It also depends on the RF settings (frequency, phase, etc.) but particularly on the scrape-off-layer (SOL) properties of the plasma, not discussed here. The ICRF coupling resistance is measured in real-time but knowledge of its parametric behaviour as function of the SOL conditions is key for tailoring the discharge to optimize the RF coupling capability (maximizing the ICRF power), e.g. by changing the plasma shape, changing the antenna phasing or injecting gas close to the antennas [21]. A similar multi-dimensional look-up table strategy as discussed for the SPA in this paper is being considered for providing the coupling resistance estimates and its improvement capabilities in real-time for the ITER control systems.

References

1. P. C. de Vries et al., Strategy to systematically design and deploy the ITER plasma control system: A system engineering and model-based design approach, Fusion Eng. and Design **204**, 114464 (2024). https://doi.org/10.1016/j.fusengdes.2024.114464
2. T. Ravensbergen et al., Strategy towards model-based design and testing of the ITER Plasma Control System, Fusion Eng. and Design, **188**, 113440 (2023). https://doi.org/10.1016/j.fusengdes.2023.113440
3. D. Karkinsky et al., Assessing NI FPGA-Based Platform With MXIe Interface for Use in ITER Hard Real-Time Investment Protection Applications, IEEE Trans. on Nucl. Science **72**, 530 (2024). http://doi.org/10.1109/TNS.2024.3474749
4. M. Schneider et al., private communications
5. D. Van Eester and R. Koch, A variational principle for studying fast-wave mode conversion, Plasma Phys. Control. Fusion **40**, 1949 (1998). https://doi.org/10.1088/0741-3335/40/11/010
6. F. Ryter et al., Experimental evidence for the key role of the ion heat channel in the physics of the L–H transition, Nucl. Fusion **54**, 083003 (2014). https://doi.org/10.1088/0029-5515/54/8/083003
7. S. Guo and F. Romanelli, The linear threshold of the ion-temperature-gradient-driven mode, Phys. Fluids **B5,** 520 (1993). https://doi.org/10.1063/1.860537
8. E. Lerche et al., Optimization of ICRH for core impurity control in JET-ILW, Nucl. Fusion **56**, 036022 (2016) https://doi.org/10.1088/0029-5515/56/3/036022
9. M Goniche et al., Ion cyclotron resonance heating for tungsten control in various JET H-mode scenarios, Plasma Phys. Control. Fusion **59**, 055001 (2017). https://doi.org/10.1088/1361-6587/aa60d2
10. J.P. Graves et al., Experimental verification of sawtooth control by energetic particles in ion cyclotron resonance heated JET tokamak plasmas, Nucl. Fusion **50**, 052002 (2010). https://doi.org/10.1088/0029-5515/50/5/052002
11. E. Lerche et al., Sawtooth control with modulated ICRH in JET-ILW H-mode plasmas, Nucl. Fusion **60**, 126037 (2020). https://doi.org/10.1088/1741-4326/abb424
12. D. Van Eester et al., Ion cyclotron resonance heating scenarios for DEMO, Nucl. Fusion **59**, 106051 (2019). https://doi.org/10.1088/1741-4326/ab318b
13. D. Van Eester, F. Louche and R. Koch, Re-evaluation of ITER ion cyclotron operating scenarios, Nucl. Fusion **42**, 310 (2002). https://doi.org/10.1088/0029-5515/42/3/312
14. M.J. Mantsinen et al., Experiments in high-performance JET plasmas in preparation of second harmonic ICRF heating of tritium in ITER, Nucl. Fusion **63**, 112015 (2023). https://doi.org/10.1088/1741-4326/aceb08
15. C. Sozzi et al., Termination of Discharges in High Performance Scenarios in JET, 28th IAEA Fusion Energy Conference (FEC 2020), Virtual, IAEA-CN-978 (2021).
16. T. H. Stix, Fast-wave heating of a two-component plasma, Nucl. Fusion **15** 737 (1975). https://doi.org/10.1088/0029-5515/15/5/003
17. D. Van Eester and E. Lerche, Simple 1D Fokker–Planck modelling of ion cyclotron resonance frequency heating at arbitrary cyclotron harmonics accounting for Coulomb relaxation on non-Maxwellian populations, Plasma Phys. Control. Fusion **53**, 092001 (2011). https://doi.org/10.1088/0741-3335/53/9/092001
18. M. Schneider et al., Simulation of heating and current drive sources for scenarios of the ITER

research plan, Nucl. Fusion **61**, 126058 (2021). https://doi.org/10.1088/1741-4326/ac34d8

19. V. Graber and E. Schuster, Nonlinear Adaptive Burn Control and Optimal Control Allocation of Over-Actuated Two-Temperature Plasmas, 2020 American Control Conference (ACC), 1411 (2020).
20. C. C. Klepper et al, Feasibility of fusion plasma burn control via real-time, sub-divertor neutral gas isotopic and compositional analysis, Nucl. Fusion 65, 086015 (2025). https://doi.org/10.1088/1741-4326/ade9dc
21. W. Zhang et al., Parametric study of midplane gas puffing to maximize ICRF power coupling in ITER, Nucl. Fusion **63**, 036008 (2023). https://doi.org/10.1088/1741-4326/acb4ad